Pergamon

PII: S0038–092X(00)00064–5

Solar Energy Vol. 67, Nos. 4–6, pp. 287–296, 1999

0038-092X/99/$ - see front matter

www.elsevier.com/locate/solener

THEORETICAL ANALYSIS AND EXPERIMENTAL RESULTS OF A 1 kW_{chem} AMMONIA SYNTHESIS REACTOR FOR A SOLAR THERMOCHEMICAL ENERGY STORAGE SYSTEM

H. KREETZ[†,1] and K. LOVEGROVE[1]

Centre for Sustainable Energy Systems, Department of Engineering, Australian National University, Canberra ACT 0200, Australia

Received 6 September 1999; revised version accepted 29 March 2000

Communicated by ARMIN RELLER

Abstract—A closed-loop solar thermochemical energy storage and transport system using the dissociation and synthesis reactions of ammonia has been investigated at the Australian National University (ANU). Work relating to the optimisation of the heat recovery part of the system is reported. Experimental investigation has shown a 1-kW_{chem} laboratory-scale ammonia synthesis reactor to operate in a stable and repeatable manner. A two-dimensional pseudo-homogeneous packed-bed catalytic reactor model previously used successfully for ammonia dissociation reactors is also confirmed to be valid for ammonia synthesis. Experiments were carried out in a closed-loop configuration and involved pressures from 9.3 to 19 MPa with internal peak reactor temperatures of up to 524°C and a constant mass flow of 0.3 $g\,s^{-1}$. A simple adjustment of intrinsic rate parameters was required to calibrate the model and reproduce the experimentally observed effects of the variation of reactor wall boundary condition and operating pressure. The investigation revealed that thermal output strongly depends on reactor wall temperature and linearly increases with operating pressure. It is now possible to predict with confidence the performance of future reactor designs. The calibrated model can also be used for detailed theoretical examination of operating strategics designed to maximise thermal and exergetic output from heat recovery reactors.

1. INTRODUCTION

A solar thermochemical energy storage system is based on the conversion of solar radiation into high-temperature heat. It consists of a closed-loop system of reactants passing alternately to endothermic 'solar' and exothermic 'heat recovery' reactors. The reactors are connected via transport lines and a gas storage container. Counterflow heat exchangers, operated in conjunction with each reactor, ensure that storage and transport operate at ambient temperature.

Solar thermochemical energy storage systems have been investigated since the 1970s and many different candidate thermochemical reactions have been considered for closed-loop and open-loop solar energy systems. In the last 10 years, carbon dioxide reforming of methane has received the most attention for solar applications (Levitan et al., 1989; Buck et al., 1991; Levy et al., 1993)

At the Australian National University (ANU) the ammonia dissociation reaction

$$NH_3 + \Delta H \Leftrightarrow 0.5N_2 + 1.5H_2 \quad (1)$$

was chosen for investigation by Carden (1974, 1977) as it is free of any secondary reactions and also offers automatic phase separation of products. A further advantage is the background of industrial experience as the 'Haber Bosch' process is nearly 100 years old. However, a theoretical disadvantage of the ammonia system is the comparably low enthalpy of reaction ($\Delta H = 66.5$ $kJ\,mol^{-1}$ compared to 247 $kJ\,mol^{-1}$ for carbon dioxide reforming of methane). The operation of an ammonia-based solar closed-loop thermochemical energy storage system is illustrated in Fig. 1.

Work on the ammonia-based system at ANU has included the examination of thermodynamic limitations (Lovegrove, 1993b), exergetic efficiency optimisation of the heat recovery part of the system (Lovegrove, 1993a; Lovegrove et al., 1999b), testing of a world-first solar-driven high-pressure ammonia dissociation reactor (Luzzi and Lovegrove, 1997) and investigation of the economics of a first-generation 10-MW_e demonstration system (Luzzi et al., 1997, 1999). In 1998 a world-first solar thermochemical closed-loop ammonia-based system was demonstrated successful-

[†]Author to whom correspondence should be addressed. Tel.: +61-2-6249-3976; fax: +61-2-6249-0506; e-mail: kreetz@faceng.anu.edu.au

[1]ISES member.

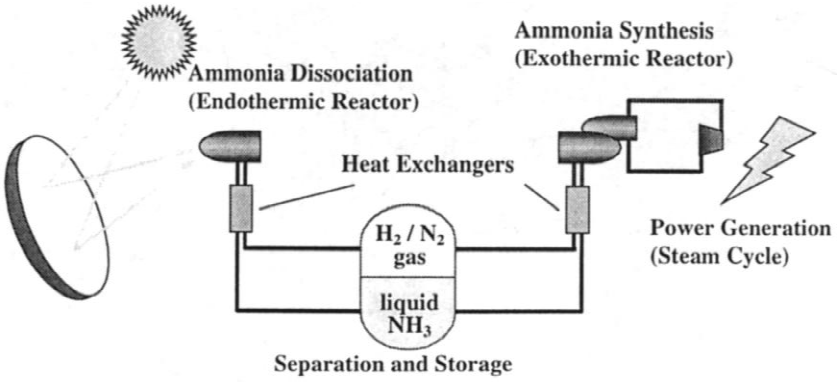

Fig. 1. Operation of a closed-loop ammonia-based solar thermochemical energy storage system.

ly (Lovegrove et al., 1999a). An associated paper (Lovegrove et al., 2000) summarises experimental results with the 1-kW_{chem} system and describes an upgraded 12–15 kW_{chem} system to accept the full input from ANU's 20-m^2 solar concentrator.

As pointed out, the industrial experience of the ammonia synthesis industry is a major advantage of the ammonia system. System components such as the synthesis reactor, heat exchanger, separator etc. which are industry standards and optimised over the last decades, could be used in a first-generation power plant. However, a separate optimisation of the closed-loop system is required as the intended purpose of components and process parameter variables is different from industrial ammonia plants. For example, the exothermic reactor would be optimised to maximise the output of high-temperature heat for electrical power generation rather than to maximise the production rate of ammonia.

This paper presents an analysis of the 1-kW_{chem} synthesis reactor used in the laboratory-scale closed-loop system. Experimental results are compared with the predictions of a two-dimensional numerical reactor model. This work is the first step towards a complete thermo-economic optimisation of synthesis reactors.

2. EXPERIMENTAL SET-UP AND METHODOLOGY

Fig. 2 shows the experimental arrangement of the solar-based closed-loop energy transfer and storage system used. Both liquid ammonia (for start up of system originally drawn from a supply vessel with 99.98% pure, anhydrous ammonia)

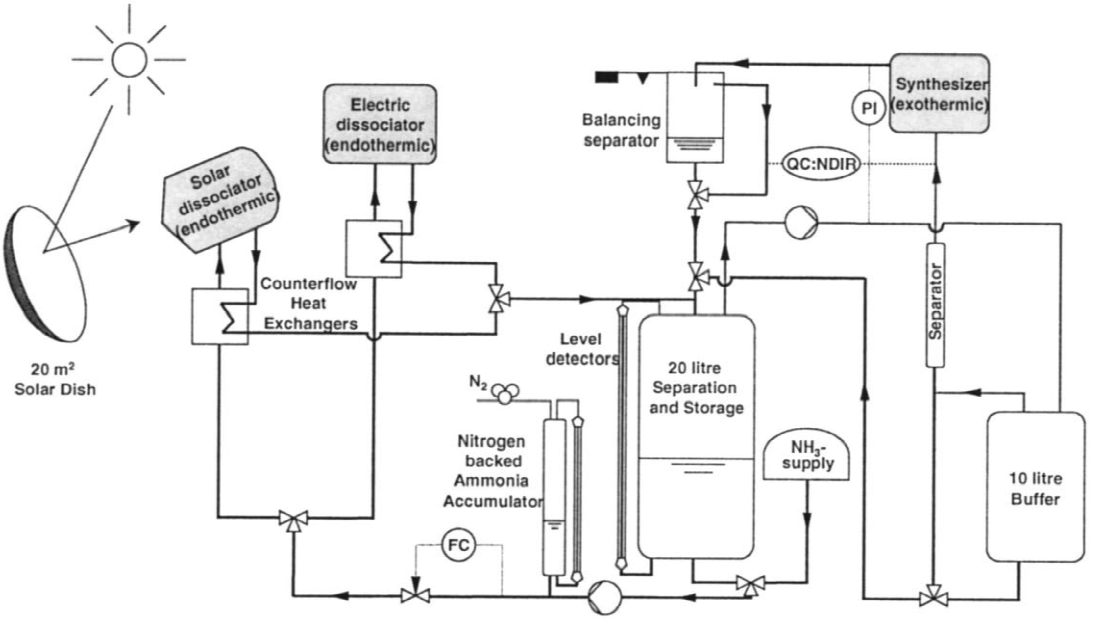

Fig. 2. Experimental arrangement of ANU's solar closed-loop energy transfer and storage system.

and the 3:1 hydrogen/nitrogen gas mixture are stored at ambient temperature and high pressure in a 20-l storage vessel. The ammonia laboratory allows handling and analysis of reactants at pressures up to 30 MPa.

The closed-loop system operates under isochoric conditions, therefore a change in pressure results from a change in molar specific volume of the gas/ammonia mixture during operation of synthesis and dissociation reactions.

For dissociation, liquid ammonia is drawn from the storage vessel and passed via a circulation pump to the nitrogen gas backed accumulator. It is subsequently passed to either an electrically heated dissociation reactor (Lovegrove, 1996) or a tubular 1-kW solar dissociation reactor. The solar reactor is an improved version of the one previously designed and tested (Luzzi and Lovegrove, 1997).

The reactor and an associated counter-flow heat exchanger are mounted on ANU's 20-m aperture paraboloidal concentrator. They are connected to the laboratory via a total of 120-m length of 1/4-inch stainless steel tubing transporting the reactants back and forth to the storage vessel at ambient temperature.

For synthesis, gas is drawn from the storage vessel by a compressor pump and stored in a 10-l buffer vessel. Subsequently, it passes through a chilled separator where some fraction of the ammonia vapour condenses and separates from the gas and travels back to the 10-l vessel. Liquid ammonia which has accumulated is periodically transferred back to the 20-l vessel. The purified gas continues on to the heat recovery reactor which is illustrated in Fig. 3.

The heat recovery reactor consists of a 1050-mm long, 21.3-mm o.d. 15.8-mm i.d. Incoloy-800 tube and is filled with Haldor Topsøe's 'KM1' triply promoted iron catalyst for the synthesis of ammonia. The catalyst was crushed, sieved and reduced using a standard industrial reduction

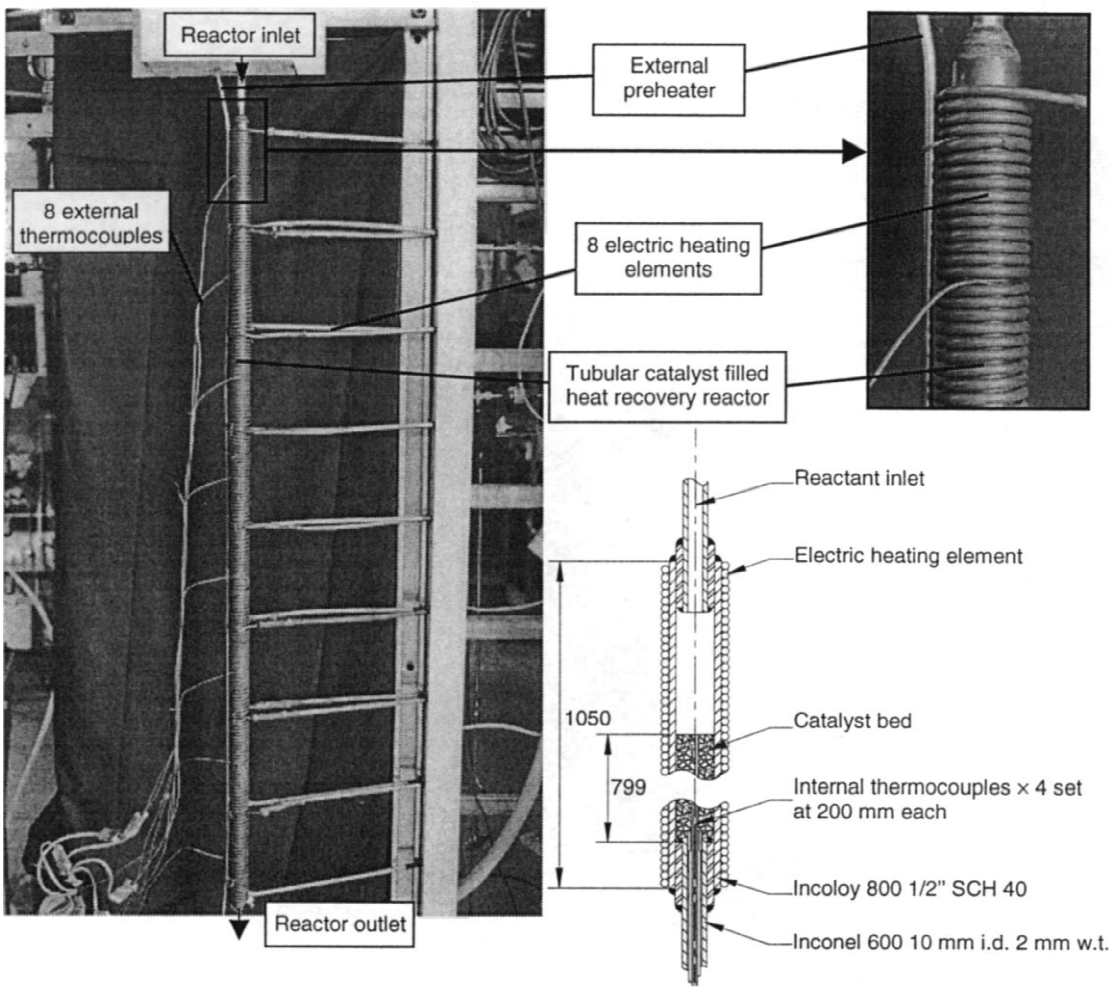

Fig. 3. The 1-kW_{chem} synthesis reactor.

Table 1. Synthesis reactor and catalyst details

Parameter	Value
Reactor dimensions	1005 mm long, 21.3 mm o.d.. 15.8 mm i.d.
Catalyst bed length	799 mm
Sieve size range of particles	1.4 to 2.36 mm
Effective particle diameter assumed	1.5 mm
Particle emissivity assumed	0.8
Void fraction	0.49±0.01 mm

procedure for promoted iron catalysts. A mixture of ammonia and 3:1 hydrogen/nitrogen gas was used as the reducing gas. Catalyst parameters are presented in Table 1.

Eight stainless steel sheathed mineral insulated heating cables made from 'Pyrotenax' 32.S.10000 material, surround the reactor, providing a maximum total heater power level of 1.94 kW_e. They are controlled by eight 'Eurotherm 808' PID feedback temperature controllers which maintain the desired external reactor wall temperature profiles irrespective of the reaction situation. During reaction, the heaters supply the heat deficit as the thermal losses from the reactor exceed the heat converted by the synthesis reaction. This setup allows investigation of various external reactor wall temperature profiles. Six stainless steel sheathed type-K thermocouple probes run up the centre of the tube to measure internal temperatures (being positioned at -72, 0, 200, 400, 600 and 836 mm from the beginning of the bed).

Incoming gas travels through a small tube external heat exchanging section which is mounted to the reactor as shown in Fig. 3. The preheated gas enters the reactor at the top and travels through another internal pre-heating section before entering the bed.

After leaving the reactor and a downstream cooler, the reactants flow to the balancing separator. It allows measurement of the mass rate of liquid accumulation during the reaction. Continuous sampling of the gas phase of the reactants is provided to a non-dispersive infra-red gas analyser (NDIR, Fisher–Rosemount model '880A') directly from the exit of the balancing separator. Zero and one hundred percent settings of the NDIR are calibrated with pure nitrogen and 99.98% anhydrous ammonia before and after each experiment. Reaction extent (mass fraction of 3:1 hydrogen/nitrogen in a gas mixture) of the exiting reactants is calculated taking into account the accumulated liquid ammonia in the balancing separator and the composition of the gas as measured by the NDIR. A correction is introduced to account for the change of balancing separator mass due to pressure changes. The net uncertainty of the reaction extent measurements of the exiting reactants stream is between 1.7 and 3.2%. The gas analyser can also take gas samples from the inlet flow to the synthesis reactor. Inlet and exit composition are measured alternately during experiments.

The mass flow of the flow stream is measured by a Fisher Rosemount Coriolis mass flow meter. Pressures are measured by semiconductor strain gauge pressure transducers and all variables are recorded every 30 s by a data logging system ('Chessel 4500') connected to a PC with analysis software (LABTECH NOTEBOOK).

Table 2 shows the nominal operating conditions used.

3. NUMERICAL MODEL

To model the behaviour of the reactor, simultaneous reaction, heat and mass transfer mechanisms have to be taken into consideration. This study used a two-dimensional pseudo-homogeneous model. The original version of this FORTRAN program was developed for tubular packed-bed steam/methane-reforming reactors and is described in detail by Richardson et al. (1988). It

Table 2. Nominal operating conditions

Parameters (range)	Nominal value/ range of operation
Fixed reactant mass flow	0.3 $g\,s^{-1}$
Pressure	9.3 to 19.0 MPa
Ambient temperature	19 to 30°C
Average external reactor temperatures	250 to 480°C
Peak internal reactor temperatures	253 to 524°C
Reactor inlet reaction extent	0.975 to 0.997
Reactor exit reaction extent	0.61 to 0.99
Time interval used for steady state averages	420 s

has been modified and validated for ammonia dissociation via extensive experiments using an electrically heated 1-kW_{chem} ammonia dissociator, as described by Lovegrove (1996). The model produces a numerical solution heavily depending on semi-empirical correlations for mass and heat transfer parameters. The catalyst bed is treated as a rotationally-symmetric 'pseudo-homogeneous' continuum not considering individual catalyst particles. Reactors with axial flow through cylindrical or annular catalyst beds can be modelled. A specification of an arbitrary temperature profile, flux profile or heat transfer fluid with the profile specified either as a polynomial or tabulated function of position along the reactor walls must be made as the boundary condition for heat transfer.

The thermodynamic data for two-phase ammonia/nitrogen–hydrogen mixtures was established by Williams (1978). Lovegrove (1996) extended this data for direct use for modelling providing additional information on thermal conductivities and viscosities taken from Vargaftik (1983). The data covers a pressure range from 10 to 30 MPa which appears to be the typical range in the ammonia converter industry (Appl, 1992a,b; Dybkjaer, 1995).

As reported by Vancini (1971), the Temkin–Pyzhev reaction rate equation can be applied to ammonia dissociation and synthesis. It is a semi-empirical equation with the chemisorption of nitrogen being the rate-determining step and is given by Eq. (2):

$$R = k_0 \cdot e^{-E_a/kT} \cdot \left(K_p^{-1} \cdot p_{N_2} \left(\frac{p_{H_2}^3}{p_{NH_3}^2} \right)^{\alpha} - \left(\frac{p_{NH_3}^2}{p_{H_2}^3} \right)^{1-\alpha} \right) \qquad (2)$$

where R is the reaction rate, $p_{reactant}$ refers to the partial pressure of the relevant reactant, α is an empirical value [typically between 0.5 and 0.724 (Vancini, 1971)], $1/kT$ is the Boltzmann factor, K_p is the equilibrium constant for the reaction, k_0 is the pre-exponential factor and E_a is the activation energy. Activation energy and pre-exponential factor were used as the main variables for fitting the model to the experimental results. Further input data comprises reactor geometry and catalyst property parameters (Table 2), mass flow, pressure and reactor wall boundary condition.

A MATLAB program has been written to accelerate the process of multiple simulation runs for parameter variations.

4. CALIBRATION OF MODEL WITH EXPERIMENTAL RESULTS

Fig. 4 shows two typical modelled and measured temperature and reaction extent profiles for

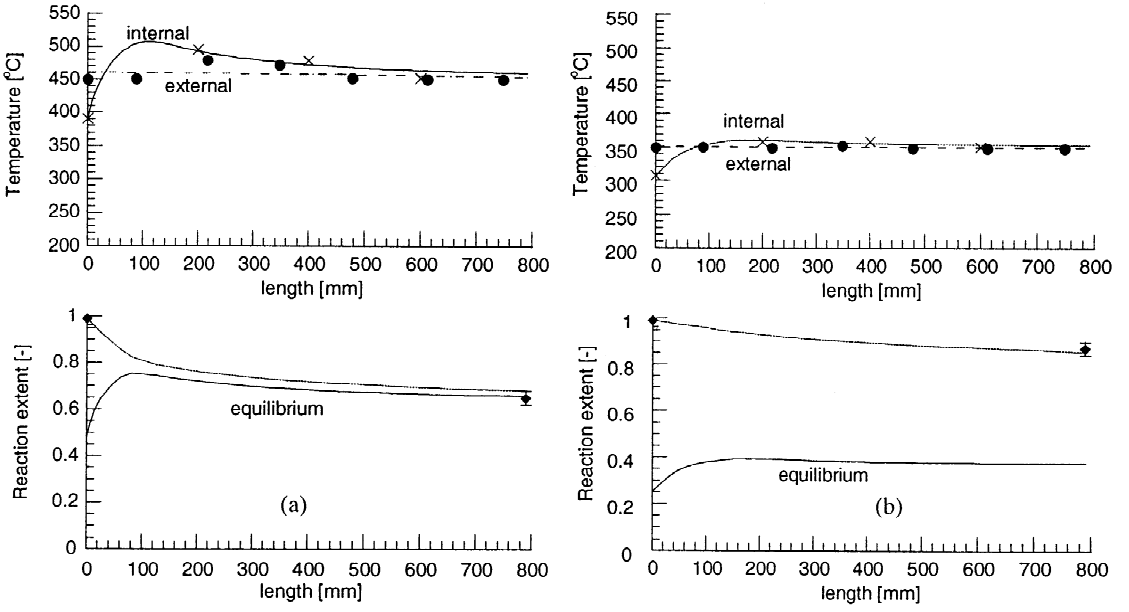

Fig. 4. Modelled internal and external reactor temperature profiles including measured internal (×) and external (●) values and modelled equilibrium and average reaction extent profiles including measured inlet and exit values (♦). Conditions: left graphs (a) 0.298±0.001 g s^{-1}, 15.04±0.29 MPa, average external reactor wall temperature 458.8°C; right graphs (b) 0.297±0.002 g s^{-1}, 14.8±0.15 MPa and 350.6°C, respectively.

nearly identical mass flows and pressures but different outer reactor wall temperature profiles. The *x*-axis represents the position in the reactor commencing at the beginning of the bed. In the bottom graphs, the equilibrium line indicates the calculated equilibrium composition corresponding to the average internal reactor temperature at each position at the given pressure.

The experimentally measured external wall temperatures show a variation from a chosen isothermal profile due to the limitations of the temperature-control system used. For input to the model, a least squares linear fit to the experimental values was used. The measured reaction extent at the inlet of the reactor, mass flow, reactor pressure and gas inlet temperature were used as inputs for the numerical model. The uncertainty in these values was found to have negligible effect on the modelled output.

For all the experimental results presented in this paper, the uncertainty of the reactant mass flow is the 0.2% quoted by the instrument manufacturer combined with the deviation from the averaged steady-state condition. The uncertainty associated with pressure measurement is the 1% calibration uncertainty combined with the deviation from averaged steady-state condition and the reaction extent measurement uncertainty is the 0.015 absolute uncertainty quoted by the instrument manufacturer combined with the deviation from averaged steady-state conditions.

Fig. 4a shows a higher change in reaction extent (more ammonia in gas) than Fig. 4b due to the higher reaction rates associated with higher operating temperatures.

The curves illustrate that a good agreement between the numerical model and the experimental results was achieved given the measured inlet reaction extent, the external reactor wall temperature profile and an adjustment of intrinsic rate parameters. The internal temperature profiles are reproduced by the model and modelled reactor exit reaction extents also correspond within the error range of the measurements.

The effect of variation of average external reactor wall temperatures on change in reaction extent between reactor inlet and exit was investigated. Fig. 5 shows the predictions by the numerical model and 11 experimental results which were carried out with a nominal pressure of 15 MPa and a nominal mass flow of 0.3 $g\,s^{-1}$. Actual operating conditions for each experimental point of Fig. 5 are presented in Table 3. A sensitivity analysis was carried out to find how measured uncertainties propagate to uncertainties in simulation results. Calculations revealed that a change in mass flow, or reaction extent of the incoming gas within their error ranges has a negligible influence

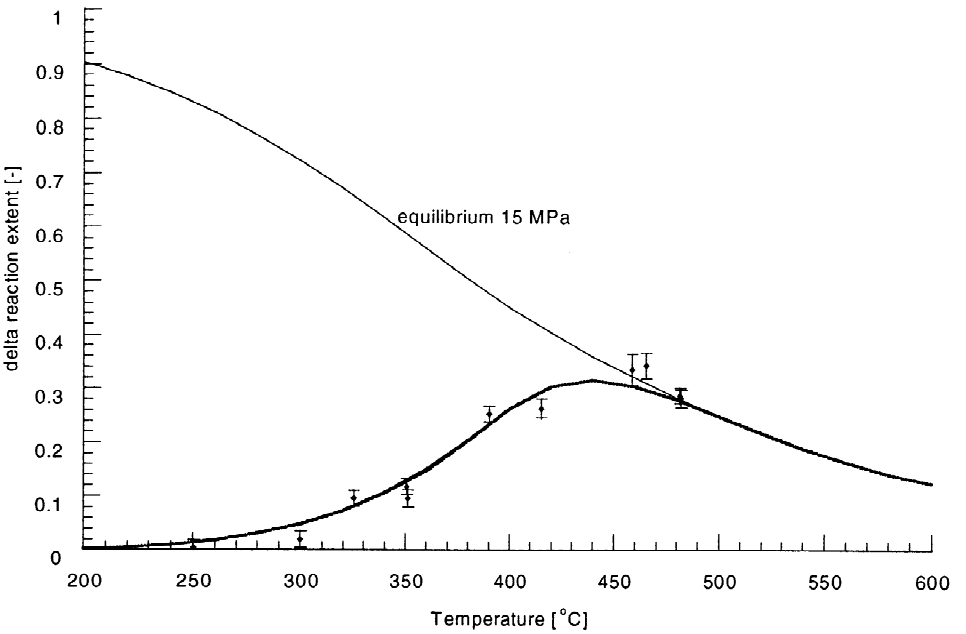

Fig. 5. The effect of variation of average external reactor wall temperatures on change in reaction extent between reactor inlet and exit, determined from numerical model and experiments. Conditions: nominal pressure: 15 MPa, nominal mass flow: 0.298 $g\,s^{-1}$.

Table 3. Actual operating conditions for each experimental point of Figs. 5 and 6

Average external reactor temperature (°C)	Pressure (MPa)	Mass flow ($g\,s^{-1}$)	Reactor inlet reaction extent
250.3	14.93±0.15	0.297±0.001	0.995±0.015
300.1	14.71±0.15	0.297±0.001	0.995±0.015
325.3	14.46±0.15	0.297±0.001	0.995±0.015
350.6	14.80±0.15	0.297±0.002	0.997±0.015
351.4	15.28±0.15	0.297±0.002	0.987±0.015
390.4	15.64±0.16	0.297±0.001	0.996±0.015
415.3	14.70±0.15	0.297±0.002	0.987±0.015
458.8	15.04±0.29	0.298±0.001	0.985±0.015
465.3	15.58±0.17	0.297±0.002	0.996±0.015
481.5	14.24±0.14	0.297±0.001	0.996±0.015
482.2	14.70±0.15	0.297±0.001	0.996±0.015

on overall results (e.g. maximum error results in a change of less than 0.5% in the change of reaction extent). The effect of pressure change within the range of the error was found to have a slight influence on the overall results, however the uncertainty associated with the experimental measurements is several times larger and no obvious correlation between deviation from modelled behaviour and deviation from nominal pressure can be seen in the results. Thus, modelling was done using overall average values. Gas inlet temperature was varied for the model by fitting the measured values to a linear function of average external wall temperature.

As already indicated by Fig. 4, an increase in average external temperature results in an increase in change of reaction extent. Generally, higher temperatures give higher reaction rates while an approach to chemical equilibrium conditions works to reduce them. Thus, maximum reaction is achieved at approximately 450°C under the conditions investigated and a further increase in average temperature results in a decrease of a change in reaction extent.

Intrinsic rate parameter values were varied in the numerical model to obtain the curve shown in Fig. 5. It represents the best overall prediction for the change in reaction extent for all experiments at this condition. A similar method of obtaining reaction extents for ammonia dissociation reactions[2] was successfully applied by Lovegrove (1996). Fig. 6 illustrates the effect of variation of activation energy for the average temperatures investigated on a change in reaction extent. For a change in activation energy, compensating changes were made for the pre-exponential factor, so that the intrinsic rate was held constant at 475°C [based on Eq. (2)]. On the basis of all the experimental results, the value determined for activation energy is 200 $kJ\,mol^{-1}$. Fig. 7 shows the effect of variation of the pre-exponential factor using the activation energy of 200 $kJ\,mol^{-1}$. The 'best-fit' value obtained by qualitatively minimizing the integrated differences between experimental and calculated points is $1.1\times10^{11}\ mol\ cm^{-3}\ atm^{-1}$.

It is generally accepted that the most accurate method for determining intrinsic rate parameters is from measurements made with plug-flow micro-reactors in which conditions are such that heat transfer and diffusion effects are insignificant (Anderson and Pratt, 1985). In the analysis reported here, the intrinsic rate parameters are effectively being used to calibrate the whole model. Since the overall results agree well with the experimental results, it is now possible to predict with confidence the performance of future reactor designs under similar conditions, particularly heat fluxes, mass fluxes and catalyst particle sizes.

Although the values of the rate parameters obtained in this way are thus not a rigorous quantification of the catalysts intrinsic properties, it is however instructive to compare them with typical values. Saladin (1998) has surveyed published values and reported activation energies for NH_3 synthesis in literature vary over a wide range between 49 and 209 $kJ\,mol^{-1}$ (Stoltze, 1995). Twigg (1989) has cited the most common figure for activation energy using triply-promoted iron catalysts for ammonia synthesis in accordance with the original Temkin Pyzhev equation (Temkin and Pyhzev, 1940) to be 158.8 $kJ\,mol^{-1}$. This suggests that the result obtained here is plausible.

An investigation of the effect of pressure was carried out with a nominal mass flow of 0.3 $g\,s^{-1}$ and wall temperature set-points of 450°C. Due to the imperfections in temperature control discussed

[2]ICI 47-1 nickel on alumina ammonia dissociation catalyst was used.

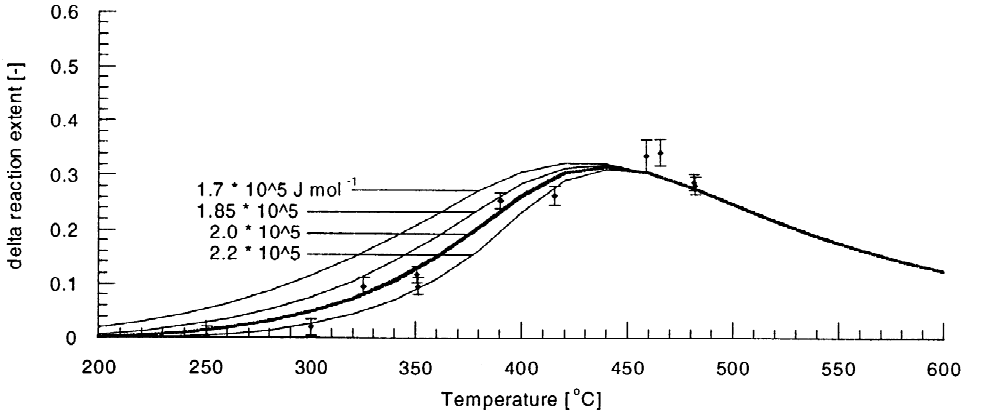

Fig. 6. The effect of variation of average external reactor wall temperatures on change in reaction extent between reactor inlet and exit determined from numerical model and experiments using different activation energies (for constant reaction rate). Conditions: nominal pressure: 15 MPa, nominal mass flow: 0.298 g s^{-1}.

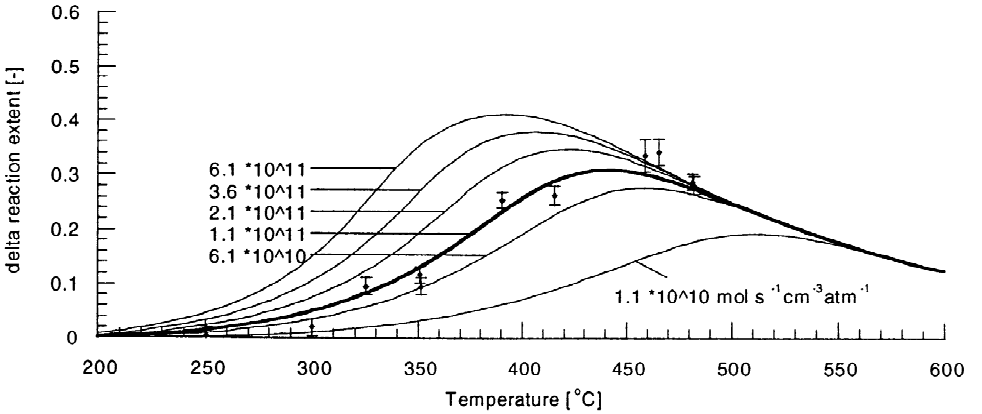

Fig. 7. The effect of variation of average external reactor wall temperatures on change in reaction extent between reactor inlet and exit determined from numerical model and experiments using different pre-exponential factors (for constant activation energy 200 kJ mol^{-1}). Conditions: nominal pressure: 15 MPa, nominal mass flow: 0.298 g s^{-1}.

previously, actual average wall temperatures varied between 450°C and 468°C. Fig. 8 shows experimental points together with model calculations made with the previously determined rate parameters (for 10, 15 and 20 MPa). Table 4 shows all actual operating conditions for each

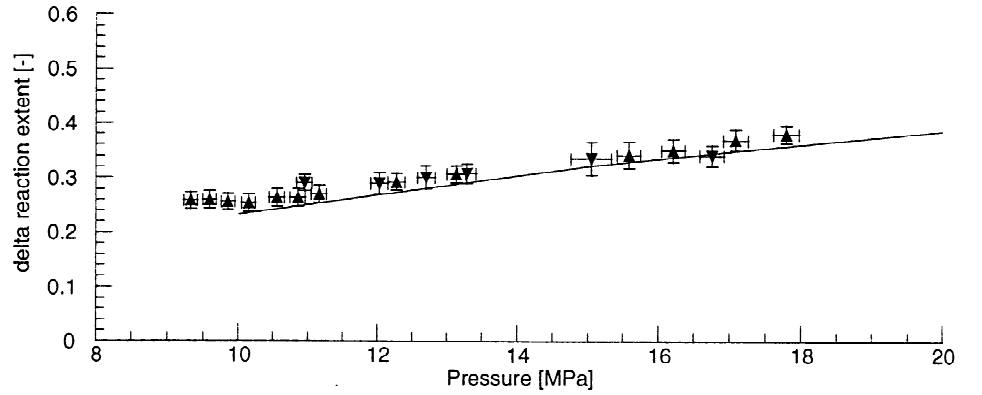

Fig. 8. The effect of variation of pressure on change in reaction extent between reactor inlet and exit determined from numerical model and experiments. Conditions: nominal mass flow: 0.298 g s^{-1} nominal average external reactor wall temperature 450°C. Experiments on 09-04-99 (▼) and 30-04-99 (▲).

Table 4. Actual operating conditions for each experimental point of Fig. 8

Average external reactor temperature (°C)	Pressure (MPa)	Mass flow ($g\,s^{-1}$)	Reactor inlet reaction extent (–)
450.8	9.32±0.09	0.297±0.003	0.996±0.015
451.1	9.58±0.09	0.297±0.003	0.996±0.015
451.3	9.85±0.1	0.297±0.002	0.996±0.015
451.5	10.15±0.1	0.297±0.002	0.996±0.015
451.7	10.55±0.11	0.297±0.004	0.996±0.015
451.8	10.85±0.11	0.296±0.004	0.996±0.015
451.9	10.95±0.11	0.297±0.001	0.985±0.015
452.0	11.16±0.11	0.298±0.001	0.996±0.015
453.5	12.03±0.12	0.297±0.001	0.985±0.015
453.6	12.28±0.12	0.297±0.001	0.996±0.015
454.5	12.70±0.13	0.297±0.001	0.985±0.015
456.1	13.13±0.13	0.297±0.002	0.996±0.015
455.3	13.29±0.13	0.290±0.001	0.985±0.015
458.8	15.04±0.29	0.298±0.001	0.985±0.015
465.3	15.58±0.17	0.296±0.002	0.996±0.015
466.1	16.21±0.16	0.295±0.006	0.985±0.015
467.8	16.76±0.17	0.298±0.001	0.996±0.015
466.3	17.09±0.17	0.297±0.002	0.996±0.015
464	17.79±0.18	0.297±0.002	0.996±0.015

experimental point of Fig. 8. As before, average values were used for modelling. Once more, the predictions of the model are in good agreement with the experimental values obtained.

The experimental points were the results of runs on two different occasions, indicated by the different symbols used. The repeatability of the experiments is obvious.

An increase of pressure results in an higher change in reaction extent and therefore in higher recovery of heat as the chemical equilibrium shifts towards lower reaction extents (in accordance with Le Chatehier's principle). Simultaneously, increasing pressure for a given mass flow increases the residence time within the bed, also working towards an increase in the amount of ammonia produced.

5. MAXIMISING OUTPUT

Figs. 5 and 8 show the effect of average external reactor wall temperature and pressure on change in reaction extent. The results indicate the relatively high sensitivity of output to the 'external reactor wall temperature'. As discussed, higher temperatures contribute to higher reaction rates while an approach to chemical equilibrium conditions works to reduce them. Thus, given a mass flow of around 0.3 $g\,s^{-1}$ and a pressure of 15 MPa, maximum reaction extent is achieved at approximately 450°C external reactor wall temperature.

Under these conditions, the change in reaction extent is 0.33. This gives a net rate of ammonia synthesis of 0.1 $g\,s^{-1}$, based on an enthalpy of reaction of 66.9 $kJ\,mol^{-1}$, this represents a heat recovery rate of 391 W. The calibrated reactor model has been used for a preliminary investigation to determine the precise choice of wall boundary conditions, reaction extent of inlet reactants and mass flow which gives maximum output for any desired operating pressure (Kreetz and Lovegrove, 1998). Based on these results, it has been found that this reactor should be capable of working at a heat recovery level of up to 1.2 kW if operated at 30 MPa, 1.3 $g\,s^{-1}$ and an average outer reactor wall temperature of 450°C.

6. CONCLUSION

This experimental investigation has shown the laboratory scale ammonia synthesis reactor and associated experimental arrangement to operate in a stable and repeatable manner. The successful experimental investigation has enabled the validity of a numerical reactor model previously used with success for ammonia dissociation reactors to be confirmed for ammonia synthesis as well. The investigation has revealed, that thermal output increases almost linearly with operating pressure. It has also shown that output depends strongly on wall temperature, with distinct maxima observable. Based on the results obtained, it can be concluded that the calibrated model is a reliable and effective tool for performance predictions for similar reactor conditions. It can also be used for a detailed theoretical examination of operating strategies designed to maximise thermal or exergetic output from heat recovery reactors.

Acknowledgements—The authors thank the German Academic

Exchange Service (DAAD) for their PhD scholarship for Holger Kreetz. We also kindly acknowledge the support of the Australian Collaborative Research Centre for Renewable Energy (ACRE), the Swiss Federal Office of Energy (BFE) and the Australian Research Council (ARC) for project support and Haldor Topsør for catalyst supply. Thanks to our colleagues Andreas Luzzi for helpful discussions and Alan Andrews for his technical assistance during the execution of this research.

REFERENCES

Anderson J. R. and Pratt K. C. (1985). *Introduction to Characterisation and Testing of Catalysts*, Academic Press, Sydney.

Appl M. (1992a) Modern Ammonia Technology — Where have we got to, where are we going? *Nitrogen* **199**, 46–75.

Appl M. (1992b) Modern Ammonia Technology — Where have we got to, where are we going? *Nitrogen* **200**, 27–53.

Buck R., Muir J., Hogan R. and Skocypec R. (1991) Carbon dioxide reforming of methane in a solar volumetric receiver/reactor: the CAESAR Project. *Solar Energy Materials* **24**, 449–463.

Carden P. O. (1974) A large scale solar plant based on the dissociation and synthesis of ammonia. In Technical Report EC-TR-8, Department of Engineering Physics. Australian National University.

Carden P. O. (1977) Energy co-radiation using the reversible ammonia dissociation reaction. *Solar Energy* **19**, 365–378.

Dybkjaer I. (1995) Ammonia Production Processes. in. In *Ammonia — Catalysis and Manufacture*, Anders Nielsen H. T. (Ed.), pp. 199–328, Springer-Verlag, Berlin, Germany.

Kreetz H. and Lovegrove K. (1998) Performance modelling of a synthesis reactor for a solar thermochemical energy storage system. In *Proceedings of 36th Annual ANZSES Conference: Solar '98, Christchurch, New Zealand*.

Levitan R., Rosin H. and Levy M. (1989) Chemical reactions in a solar furnace — direct heating of the reactor in a tubular receiver. *Solar Energy Materials* **24**, 464–477.

Levy M., Levitan R., Rosin H. and Rubin R. (1993) Solar energy storage via a closed loop chemical heat pipe. *Solar Energy* **50**, 179.

Lovegrove K., Luzzi A. and Kreetz H. (2000). A solar driven ammonia-based thermochemical energy storage system. *Solar Energy*. In press.

Lovegrove K. (1993a) Exergetic optimisation of a solar thermochemical energy storage system subject to real constraints. *Int. J. Energy Res.* **17**, 831–845.

Lovegrove K. (1993b) Thermodynamic limits on the performance of a solar thermochemical energy storage system. *Int. J. Energy Res.* **17**, 817–829.

Lovegrove K. (1996) High pressure ammonia dissociation experiments for solar energy transport and storage. *Int. J. Energy Res.* **20**, 965–978.

Lovegrove K., Kreetz H. and Luzzi A. (1999a) The first ammonia-based solar thermochemical energy storage demonstration. *J. de Physique IV* **9**, 581–586.

Lovegrove K., Luzzi A., McCann M. and Freitag O. (1999b) Exergy analysis of ammonia-based solar thermochemical power systems. *Solar Energy* **66**, 103–115.

Luzzi A., Lovegrove K., Filipi E., Fricker H., Schmitz-Goeb M. and Chandapillai M. (1997) Base-load solar power using the 'Haber-Bosch' process. In *Project Report Number 59312*, Bundesamt für Energie (BFE), 3003 Bern, Switzerland.

Luzzi A. and Lovegrove K. (1997) A solar thermochemical power plant using ammonia as an attractive option for greenhouse-gas abatement. *Energy* **22**, 317–325.

Luzzi A., Lovegrove K., Filippi E., Fricker H., Schmitz-Goeb M. and Chandapillai M. et al. (1999) Techno-Economic analysis of a 10 MW_e solar thermal power plant using ammonia-based thermochemical energy storage. *Solar Energy* **66**, 91–101.

Richardson J. T., Paripatyadar S. A. and Shen J. C. (1988) Dynamics of a sodium heat pipe reforming reactor. *AIChE J.* **34**, 743–752.

Saladin F. (1998) A micro-reactor for the measurement of intrinsic rate data of the catalytic dissociation and synthesis of ammonia at high temperatures and pressures. In *Technical Report*, Department of Engineering, Australian National University.

Stoltze P. (1995) Structure and surface chemistry of industrial ammonia synthesis catalysts. In *Ammonia — Catalysis and Manufacture*, Anders Nielsen H. T. (Ed.), pp. 17–102, Springer-Verlag, Berlin, Germany.

Temkin M. and Pyhzev V. (1940). *Acta Physicochim. U.R.S.S.* **12**, 327.

Twigg M. (1989). Catalyst Handbook, Vol. 2, Wolfe Publishing, London, UK.

Vancini C. A. (1971). *Synthesis of Ammonia*, The Macmillan Press, London.

Vargaftik N. B. (1983). *Handbook of Physical Properties of Liquids and Gases: Pure Substances and Mixtures*, Hemisphere Publishing.

Williams O. M. (1978) Generation of thermochemical energy transfer data for the ammonia/hydrogen–nitrogen system. In *Technical Report 16*, Department of Engineering Physics, Australian National University.